THERMOPHYSICAL PROPERTIES OF ZIRCONIUM
AT HIGH TEMPERATURE

Paul-François Paradis and Won-Kyu Rhim

Jet Propulsion Laboratory, California Institute of Technology

4800 Oak Grove Drive, Pasadena, CA 91109

(02/02/99)

ABSTRACT

Six thermophysical properties of both the solid and liquid zirconium measured using the high-temperature electrostatic levitator at JPL are presented. These properties are: density, thermal expansion coefficient, constant pressure heat capacity, hemispherical total emissivity, surface tension and viscosity. For the first time, we report the densities and the thermal expansion coefficients of both the solid as well as liquid Zr over wide ranges of temperatures.

Over the 1700 ~ 2300 K temperature span, the liquid density can be expressed as $\rho_l(T) = 6.24 \times 10^3 - 0.29 (T - T_m)$ kg/m^3 with $T_m = 2128$ K, and the corresponding volume expansion coefficient as $\alpha_l = 4.6 \times 10^{-5}$ /K. Similarly, over the 1250 ~ 2100 K range, the measured density of the solid can be expressed as $\rho_s(T) = 6.34 \times 10^3 - 0.15 (T - T_m)$, giving a volume expansion coefficient $\alpha_s = 2.35 \times 10^{-5}$ /K.

The constant pressure heat capacity of the liquid phase could be estimated as $C_{pl}(T) = 39.72 - 7.42 \times 10^{-3} (T - T_m)$ J/mol/K if the hemispherical total emissivity of the liquid phase ε_{Tl} remains constant at 0.3 over the 1825 ~ 2200 K range. Over the 1400 ~ 2100 K temperature span, the hemispherical total emissivity of the solid phase could be rendered as $\varepsilon_{Ts}(T) = 0.29 - 9.91 \times 10^3 (T - T_m)$.

The measured surface tension and the viscosity of the molten zirconium over the 1850 ~ 2200 K range can be expressed as $\sigma(T) = 1.459 \times 10^3 - 0.244 (T - T_m)$ mN/m and as $\eta(T) = 4.83 - 5.31 \times 10^{-3}(T - T_m)$ mPa.s, respectively.

I. INTRODUCTION

An accurate knowledge of thermophysical properties is important for various fundamental studies on phase transformations and nucleation, as well as industrial processes on metals, such as refining, forming and casting. In some cases, the properties can be used to determine other thermodynamic parameters. For instance, enthalpy, entropy, and the Gibbs free energy can be derived from the heat capacity. The present paper focuses on the thermophysical properties of both the solid and liquid zirconium at high temperature. The properties include density, thermal expansion coefficient, constant pressure heat capacity, total hemispherical emissivity, surface tension and viscosity. Zirconium is widely used for various applications because of its refractory nature, its resistance to corrosive chemical environments (acids, alkalis, sea water, etc.), and its low neutron absorption cross section [1]. However, its high melting point and the risk of contamination in its molten phase make it difficult to measure its thermophysical properties using traditional methods and hence, necessitates the use of a containerless technique. The advent of the electrostatic levitation, and the recent development of non-contact diagnostic techniques, circumvent these difficulties, allowing an accurate and quick determination of the thermophysical properties [2-7]. Our experimental facility allowed us to levitate a sample in a high vacuum, and to process it at high temperature using laser radiation, thus isolating it from contaminating container walls as well as surrounding gasses.

II. EXPERIMENTAL SET-UP AND PROCEDURES

The measurements reported in this paper have been done using the high-temperature electrostatic levitator (HTESL) at the Jet Propulsion Laboratory [2]. Figure 1 shows a schematic diagram of the HTESL. The sample and electrodes were housed in a stainless-steel chamber which was typically evacuated to 10^{-8} Torr before heating began. For these measurements, samples with diameters close to 2.5 mm were used. The material, zirconium of 99.95 % purity, came from Teledyne Wah-Chang, Albany, Oregon. The

HTESL achieved sample positioning between the parallel plate electrodes using a feedback control system. This system relied on He-Ne lasers that projected sample images on position detectors. Typically, the top and bottom electrodes were spaced 12 mm apart (fig. 2). The sample rotation rate was measured by detecting the reflected He-Ne laser beam from its surface. A 1-kW xenon arc lamp was used for initial sample heating, until thermionic emission regime was attained. Then, the sample was heated further and melted using a Nd-YAG laser. For these experiments, temperatures in excess of 2300 K were reached.

Once molten as shown in figure 3, the levitated sample assumed a nearly spherical shape, thanks to the action of surface tension. Moreover, since the electrostatic levitation scheme did not transfer any heat to the sample, a heated sample cooled purely radiatively when the cooling was initiated by blocking the laser beam. The energy equation describing the cooling process is given by:

$$\frac{m}{M} C_p \frac{dT}{dt} = -\varepsilon_T A \sigma_{SB} (T^4 - T_a^4) \tag{1}$$

where m is the sample mass, M the atomic weight, C_p the molar heat capacity at constant pressure, T_a and T are respectively the ambient and sample temperatures, ε_T the hemispherical total emissivity, A the surface area of the sample, and σ_{SB} the Stefan-Boltzmann constant (5.6705×10^{-8} W.m^{-2}.K^{-4}).

The temperature was measured using a single color custom-made pyrometer operating at 750 nm and was then digitized and calibrated using a LabView software. Since the heating was achieved with a laser at 1.06 μm, the risks of spectral interference were avoided. The emissivity of the sample was determined with respect to the melting temperature (2128 K) and was assumed constant throughout cooling. A typical cooling curve showing undercooling and recalescence is depicted in figure 4.

The simultaneous measurement of both the density and the heat capacity over temperature was initiated after the laser beam had been blocked and the sample allowed to cool. To measure the density, video images were recorded during the cooling process. In our case, the sample was axisymmetric and only a side view was needed (fig. 3). The recorded images were digitized and the sample area was extracted from each video frame using an analysis software developed at JPL [5]. The volume could then be calculated, and, knowing the mass of the sample, the density was found. Finally, the temperature time dependency was extracted from the cooling curve and was correlated with video frames allowing the density to be expressed as a function of temperature.

The ratio of heat capacity over hemispherical total emissivity was found as a function of temperature using equation (1) since all other parameters were known. The temperature-time dependency (dT/dt) was extracted from the cooling curve (fig. 4) and the sample area was found from the video images.

To measure the surface tension and the viscosity, a $P_2\cos(\theta)$-mode drop oscillation was induced by superimposing a small sinusoidal electric field on the levitation field (fig. 2). The transient signal which followed the termination of the excitation field was detected, recorded, and analyzed using a LabView software. A typical signal of the decay of the oscillation is shown in figure 5. This was done several times for a given temperature and repeated for few temperatures. Using the characteristic oscillation frequency ω_c of this signal after correcting for non uniform surface charge distribution [8], the surface tension σ can be extracted from the following equation [7]:

$$\omega_c^2 = \frac{8\sigma}{r_o^3\rho}\left(1 - \frac{Q^2}{64\pi^2 r_o^3\sigma\varepsilon_o}\right)[1 - F(\sigma,q,e)], \tag{2}$$

where

$$F(\sigma,q,e) = \frac{\left(243.31\sigma^2 - 63.14q^2\sigma + 1.54q^4\right)e^2}{176\sigma^3 - 120q^2\sigma^2 + 27\sigma q^4 - 2q^6}, \tag{3}$$

5

where r_0 is the radius of the sample when it assumes a spherical shape, ρ is the liquid density, Q is the drop charge, ε_0 the permittivity of vacuum, and q and e are defined by:

$$q^2 \equiv \frac{Q^2}{16\pi^2 r_o^3 \varepsilon_o}, \tag{4}$$

and

$$e^2 \equiv E^2 r_o \varepsilon_o, \tag{5}$$

respectively, E being the applied electric field. Similarly, using the decay time τ given by the same signal (fig. 5), the viscosity η is found by:

$$\eta = \frac{\rho r_o^2}{5\tau}. \tag{6}$$

The theory of this method, the hardware, and software used have been described in detail elsewhere [7].

III. RESULTS AND DISCUSSION

A. Density

The results of our density measurements for liquid zirconium are shown in figure 6. The measurements were taken over the 1700 ~ 2300 K temperature range thus covering the undercooled region by as much as 300 K. As that of other pure metals, the density of zirconium exhibits a linear nature as a function of temperature and can be fitted by the following equation:

$$\rho_l(T) = 6.24 \times 10^3 - 0.29\,(T - T_m) \quad kg/m^3 \qquad (1700 \sim 2300\ K), \tag{7}$$

where T_m is the melting temperature (2128 K). In this experiment, the accuracy of the measurements was estimated to be ±0.5%. To our knowledge, these measurements were

the first reported on such temperature range. Most of the values that appear in various references are given in the vicinity of the melting point and they vary substantially. Peterson et al [9] estimated it as 5.5×10^3 kg/m^3, Eljutin et al. [10] measured it as 5.6×10^3 kg/m^3, Maurakh [11] determined it as 6.06×10^3 kg/m^3 (1875 K) and Allen calculated it as 5.80×10^3 kg/m^3 [12]. Our value is 11% larger than that estimated by Peterson et al but only 3% greater than that measured by Maurakh. Also, our temperature coefficient is smaller by 9% compared to that estimated by Steinberg [13].

The volume variation $V_l(T)$ of the molten state, normalized with the volume at the melting point V_m, can be derived from equation (7), and be fitted with the following equation:

$$V_l(T)/ V_m = 1 + 4.6 \times 10^{-5}(T - T_m), \qquad (8)$$

where $4.6 \times 10^{-5} K^{-1}$ represents the volume expansion coefficient.

The observed discrepancies between our results and those of Eljutin et al and Maurakh could be attributed to the difference in processing techniques. We used a containerless approach isolating our samples from container walls, whereas the above authors used traditional schemes for which possible chemical reactions between the highly reactive molten zirconium and crucibles could have altered the final density values.

Figure 6 also shows the density measurements for the solid phase over the 1250 ~ 2100 K temperature range. Again, a linear behavior is observed and the data can be fitted by the following equation:

$$\rho_s(T) = 6.34 \times 10^3 - 0.15 (T - T_m) \quad kg/m^3 \qquad (1250 \sim 2100 \ K). \qquad (9)$$

These are the first data to be reported on the density of solid zirconium over a wide range of high temperatures. Our value for the density of the solid at the melting temperature

compares well with those found in the literature. Our density is only 1% smaller than that reported by Peterson et al, 1.6% smaller than that of Schaffer [14], and 2.6% higher than the one given in reference [1].

From equation (9), the volume variation $V_s(T)$ of the solid, normalized with the volume at melting temperature V_m, can be derived and satisfies the following equation:

$$V_s(T)/V_m = 1 + 2.35 \times 10^{-5}(T - T_m), \tag{10}$$

where 2.35×10^{-5} represents the volume expansion coefficient α_s (K^{-1}). To our knowledge, this is the first time that this value is reported.

As can be seen in figure 6, there is a discontinuity in density at the melting point, characteristic of a first order transition. The figure also reveals a crossing point (~ 1415 K) between the solid curve and the extrapolated liquid curve. This point, being 713 K below the melting temperature and 385 K below the heterogeneous nucleation limit achieved in these experiments, may correspond to the undercooling limit before the homogeneous nucleation comes into effect. To further reduce heterogeneous nucleation, undercooling experiments with samples smaller than the one used for the present experiments ($<< 2$mm) are being planned.

B. Constant-Pressure Heat Capacity

The ratio between constant-pressure heat capacity and hemispherical total emissivity as a function of temperature is shown in figure 7 for both solid and liquid zirconium. For the liquid state, $C_{pl}(T)/\varepsilon_{Tl}$ exhibits a slight decreasing trend with increasing temperature and can be fitted as:

$$C_{pl}(T)/\varepsilon_{Tl} = 132.28 - 2.65 \times 10^{-2} (T - T_m) \quad \text{J/mol/K} \quad (1825 \sim 2200 \text{ K}). \tag{11}$$

Our values of $C_{pl}(T)/\varepsilon_{Tl}$ agree within a few percent to those reported by Rulison and Rhim [4]. If the value of $C_{pl} = 40.7$ J/mol/K given by Bonnell [15] at the melting temperature is used, the ε_{Tl} that can be determined from equation (11) is given by $\varepsilon_{Tl} = 0.3$ at that temperature. Then, assuming that ε_{Tl} remains to be constant at 0.3 over the temperature range, the temperature dependency of C_{pl} can be determined from equation (11) by simply multiplying by $\varepsilon_{Tl} = 0.3$. The heat capacity so obtained (fig. 8) can be expressed by the following equation:

$$C_{pl}(T) = 39.72 - 7.42 \times 10^{-3} (T - T_m) \quad \text{J/mol/K} \qquad (1825 \sim 2200 \text{ K}). \qquad (12)$$

Figure 7 also gives the variation of C_{ps}/ε_{Ts} as a function of temperature for high temperature solid zirconium. The ratio can be expressed as:

$$C_{ps}(T)/\varepsilon_{Ts} = 123.42 - 1.51 \times 10^{-2} (T - T_m) \quad \text{J/mol/K} \quad (1400 \sim 2100 \text{ K}). \qquad (13)$$

Cezairliyan and Righini [16] measured $C_{ps}(T)$ and $\varepsilon_{Ts}(T)$ using a pulse heating technique. According to these authors, their results of $C_{ps}(T)$ are more reliable than those for their $\varepsilon_{Ts}(T)$. Using their value of $C_{ps}(T)$ and our value of $C_{ps}(T)/\varepsilon_{Ts}$ (fig. 7), it is possible to estimate ε_{Ts} as a function of temperature (fig. 9). The hemispherical total emissivity so obtained can be fitted as:

$$\varepsilon_{Ts}(T) = 0.29 - 9.91 \times 10^3 (T - T_m) \qquad\qquad (1400 \sim 2100 \text{ K}). \qquad (14)$$

At the melting point, the value of ε_{Ts} so obtained is 14% lower than that reported by Cezairliyan and Righini and 9% higher than that reported by Zhorov [17]. The present coefficient is 16% higher than that reported by Cezairliyan and Righini and nearly twice higher than that reported by Zhorov. The above discrepancies may be attributable to

differences in sample surface conditions. As the samples solidified from deeply undercooled liquid states, the smooth surface condition seemed to have preserved. This is probably due to the fact that the solids resulting from deeply undercooled liquids tends to produce fine micro-structures, leading to a smooth surface [18]. Cezairliyan and Righini, however, noticed during their work that the initial smooth surface of their sample changed to an uneven rough surface as a result of repeated heating and cooling. This may partially account for their higher values of emissivity.

C. Surface Tension and Viscosity

For completeness, the results of the measurements of surface tension and viscosity of molten zirconium are presented. By assembling the frequency data drawn from many signals similar to those of figure 5, it was possible to create figure 10. This figure depicts the surface tension of a molten sample over the 1850 ~ 2200 K temperature span, thus extending the measurements into the undercooled region. Note that the surface tension at 1860 and 1960 K comprises two data points each. The linear fit of the data could satisfy the following equation:

$$\sigma(T) = 1.459 \times 10^3 - 0.244 \, (T - T_m) \text{ mN/m} \qquad (1850 \sim 2200 \text{ K}). \qquad (15)$$

Our surface tension datum at melting point agrees very well with that of Flint (1457 mN/m)[19] and is within 2% to that reported by Allen (1480 mN/m)[20]. These discrepancies could be attributed to the difference in processing techniques. We used a containerless approach whereas the above authors used traditional schemes, more prone to surface contamination. Our levitated molten samples showed no oxide patches or any other structures on their entire surface, and they undercooled as much as 300 K when they were allowed to cool freely. The melting temperature of Zr being 2128 K, the impurities and

oxides on the sample surface seemed to have been either evaporated or dissolved at high temperature.

Frohberg et al. recently used an electromagnetic levitator and measured surface tension of pure zirconium both on the ground and in the low gravity environment of the Space Shuttle [21]. Their ground and microgravity results can be expressed respectively by:

$$\sigma_{1g}(T) = 1.543 \times 10^3 - 0.66\,(T - T_m) \text{ mN/m} \qquad (2000 \sim 2250 \text{ K}). \qquad (16)$$

$$\sigma_{\mu g}(T) = 1.512 \times 10^3 - 0.37\,(T - T_m) \text{ mN/m} \qquad (1950 \sim 2200 \text{ K}). \qquad (17)$$

At the melting point, their space result is about 3.6% larger than ours, and their ground result is larger than ours by 5.7%. Their temperature coefficients are at least 50% larger than ours. According to Chen and Overfelt [22], the magnetic field, used in electromagnetic levitation, causes a slight increase in the stiffness of the drop raising the apparent surface tension. This effect may be more pronounced for larger samples since they feel a stronger magnetic pressure. Probably, this reason would account for the discrepancies.

By taking the decay time components from the same data points used to determine surface tension, it was possible to generate figure 11 over the same temperature interval (1850 ~ 2200 K). The figure illustrates the viscosity of a molten sample versus temperature. The data could be expressed as:

$$\eta(T) = 4.83 - 5.31 \times 10^{-3}(T - T_m) \text{ mPa.s} \qquad (1850 \sim 2200 \text{ K}). \qquad (18)$$

Here again, the viscosity at 1860 and 1960 K comprises two data points each. To the best of our knowledge, our results for viscosity were the first ones to be reported. Both the viscosity and surface tension data were extensively discussed in an earlier paper [7].

11

IV. CONCLUSION

We have presented several thermophysical properties of solid and liquid zirconium, measured using the high temperature electrostatic levitator (HTESL) at JPL. For the first time, we reported the densities and the thermal expansion coefficients of solid as well as liquid phases over wide temperature ranges. The measurements for the liquid phase were extended up to 300 K into the undercooled region. We also presented results on viscosity which have never been reported by other researchers. Our results of surface tension and constant pressure heat capacity of molten Zr as well as those of the hemispherical total emissivity of the solid phase complemented the scarce data that can be found in the literature.

All the thermophysical properties presented were determined or derived from cooling curves and images acquisition. Therefore, to improve our data, efforts should still be directed onto ways to increase image sharpness, resolution, and contrast. Efforts should also be put in new numerical techniques to determine dT/dt from the cooling curves to diminish numerically induced errors .

As a final note, we would like to mention that our facility also possesses the capability to determine the spectral emissivity and the electrical conductivity [6]. Some instrument modifications are currently underway to implement these capabilities to zirconium, and the results will be published elsewhere.
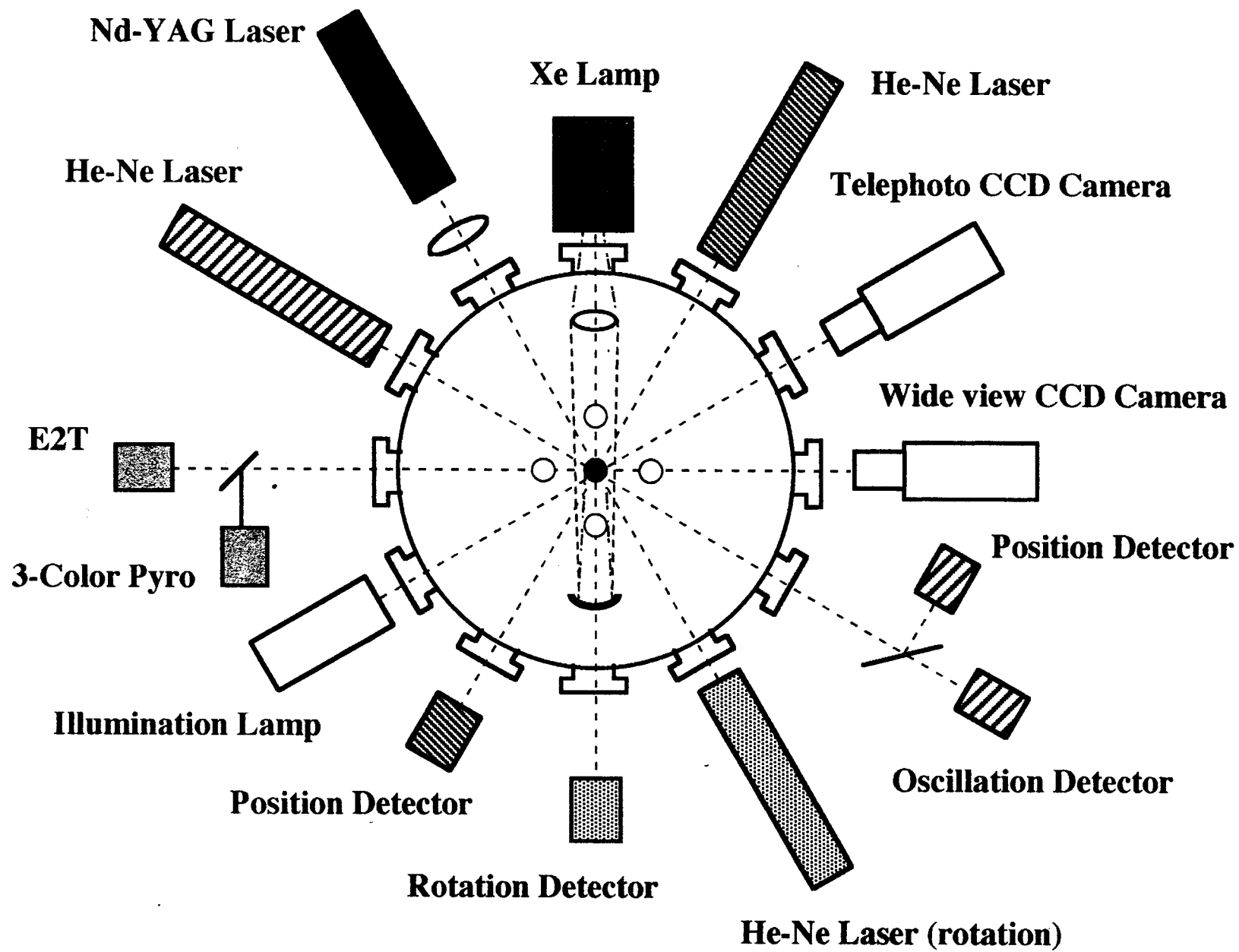
REFERENCES

[1] *CRC Handbook of Chemistry and Physics*, 62nd ed., edited by R.C. Weast and M.J. Astle (CRC, Boca Raton, FL, 1981).

[2] W.-K. Rhim, S.K. Chung, D. Barber, K.F. Man, G. Gutt, A. Rulison, and R.E. Spjut, Rev. Sci. Instrum. **64**, 2961 (1993).

[3] A.J. Rulison and W.-K. Rhim, Rev. Sci. Instrum. **65**, 695 (1994).

[4] A.J. Rulison and W.-K. Rhim, Metall. Mater. Trans. B. **26B**, 503 (1995).

[5] S.K. Chung, D.B. Thiessen, and W.-K. Rhim, Rev. Sci. Instrum. **67**, 3175 (1996).

[6] W.-K. Rhim and T. Ishikawa, Rev. Sci. Instrum. **69**, 3628 (1998).

[7] W.-K. Rhim, K. Ohsaka, P.-F. Paradis, and R.E. Spjut, (submitted for publication, Rev. Sci. Instrum. Nov. 1998).

[8] J.Q. Feng and K.V. Beard, Proc. Roy. Soc. (London), A, **430**, 133 (1990).

[9] A.W. Peterson, H. Kedesdy, P.H. Keck, and E. Scharz, J. Appl. Phys. **29**, 213 (1958).

[10] Eljutin, Kostikov, and Penkow, Poroshk. Met., **9**, 46 (1970).

[11] M.A. Maurakh, Trans. Indian Inst. Met., **14**, 209 (1964).

[12] B.C. Allen, Trans. AIME, **227**, 1175 (1963).

[13] D.J. Steinberg, Metall. Trans. **5**, 1341 (1974).

[14] Schaffer, P.T.B., Plenum Press Handbook of High Temperature Materials Index (Plenum Press, New-York 1964).

[15] D.W. Bonnell, Ph.D. thesis, Rice University, 1972.

[16] A. Cezairliyan and F. Righini, J. Res. N.B.S. A **78A**, 509 (1974).

[17] G.A. Zhorov, High Temp. **8**, 501 (1970).

[18] J.L. Walker, *The physical chemistry of process metallurgy*, Part 2, edited by G.R. St-Pierre (Interscience, New-York, 1959).

[19] O. Flint, J. Nucl. Instrum. **16**, 260 (1965).

[20]   B.C. Allen, The Surface Tension of Liquid Metals, *in Liquid Metals: chemistry and physics*, edited by S.Z. Beer (Marcel Dekker, New-York, NY, 1972).

[21]   M.G. Frohberg, M. Roesner-Kuhn, and G. Kuppermann: "Measurements of the surface tension of liquid and undercooled metallic alloys by oscillating drop technique", *in International Workshop on Nucleation and Thermophysical Properties of Undercooled Melts*, Physikzentrum Bad Honnef, March 4-6, 1998.

[22]   S.-F. Chen, and R.A. Overfelt, Int. J. Thermophys., **19** (3) 817 (1998).

FIGURE CAPTIONS

Figure 1.   Schematic diagram of the high-temperature electrostatic levitator.

Figure 2.   Schematic arrangement of the electrode assembly.

Figure 3.   Image of a molten, levitating zirconium sample.

Figure 4.   Radiative cooling curve, exhibiting deep undercooling and recalescence plateau.

Figure 5.   Signal of the decay of the oscillation of a zirconium sample (mass: 39.6mg; oscillating frequency: 185.20 Hz; decay constant: 0.3651 s).

Figure 6.   Density of zirconium versus temperature, obtained from video image analysis and cooling curve data.

Figure 7.   Ratio between constant-pressure heat capacity and total hemispherical emissivity of zirconium versus temperature.

Figure 8.   Heat capacity of zirconium versus temperature. In the case of the liquid, $C_{pl}(T)$ has been calculated using data from figure 7 and $\varepsilon_{Tl} = 0.3$.

Figure 9.   Hemispherical total emissivity ε_{Ts} as a function of temperature estimated using data from figure 7 and $C_{ps}(T)$ from reference [16].

Figure 10.   Surface tension of a molten zirconium sample versus temperature. The curve was created by assembling the frequency data drawn from many signals similar to that of figure 5. Note that the surface tension at 1860 and 1960 K comprises two data points each.

Figure 11.   Viscosity of a molten zirconium sample versus temperature. The curve was created by assembling the decay time data drawn from many signals similar to that of figure 5. Note that the viscosity at 1860 and 1960K comprises two data points each.
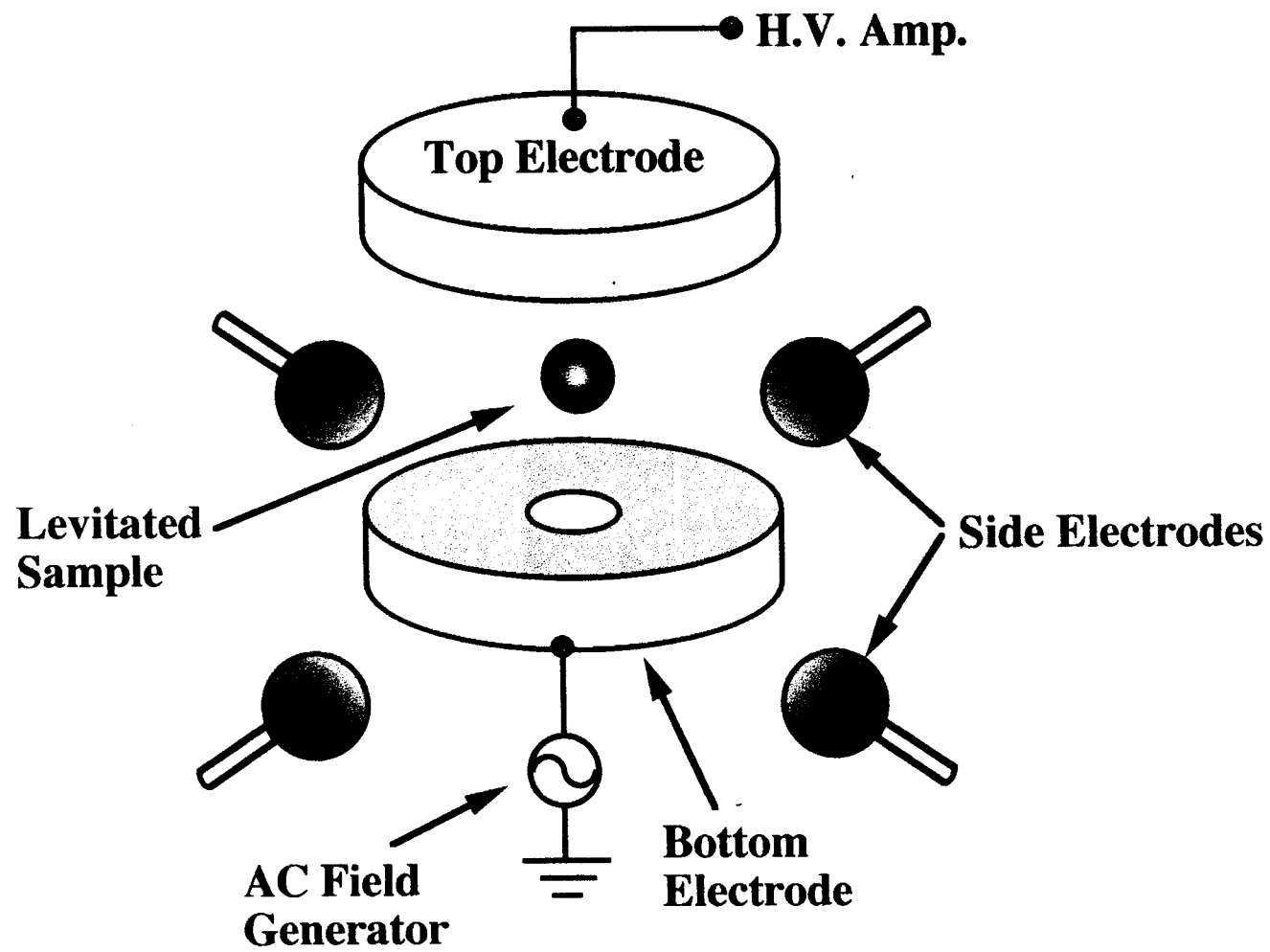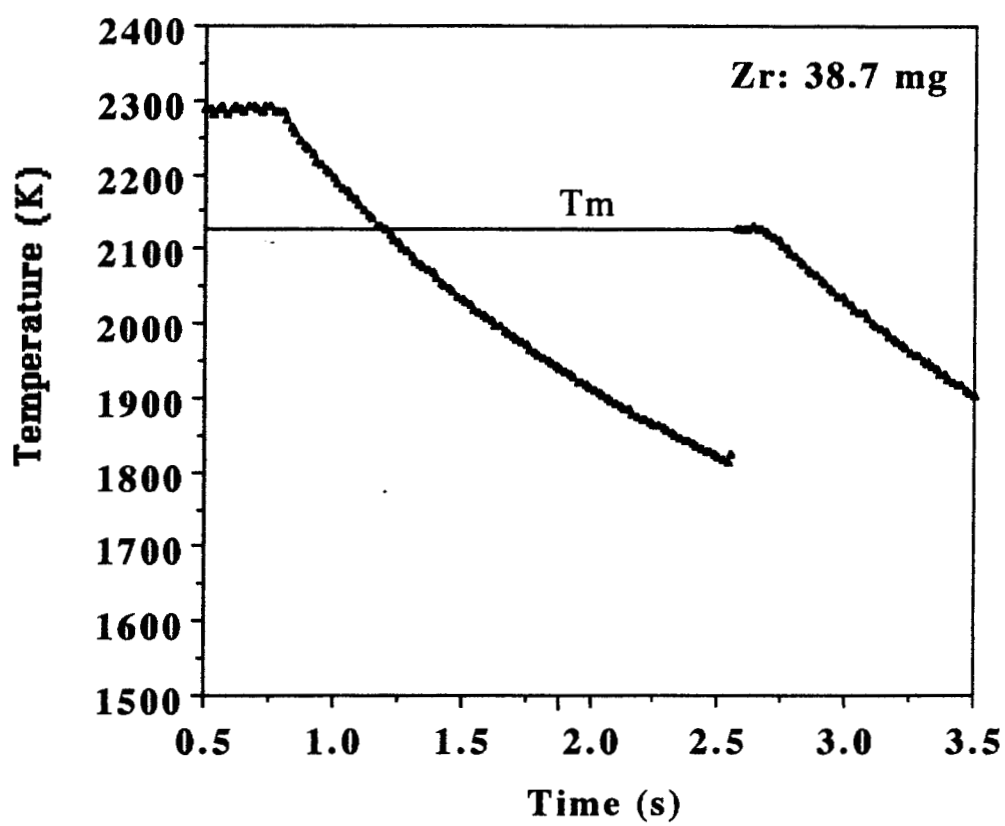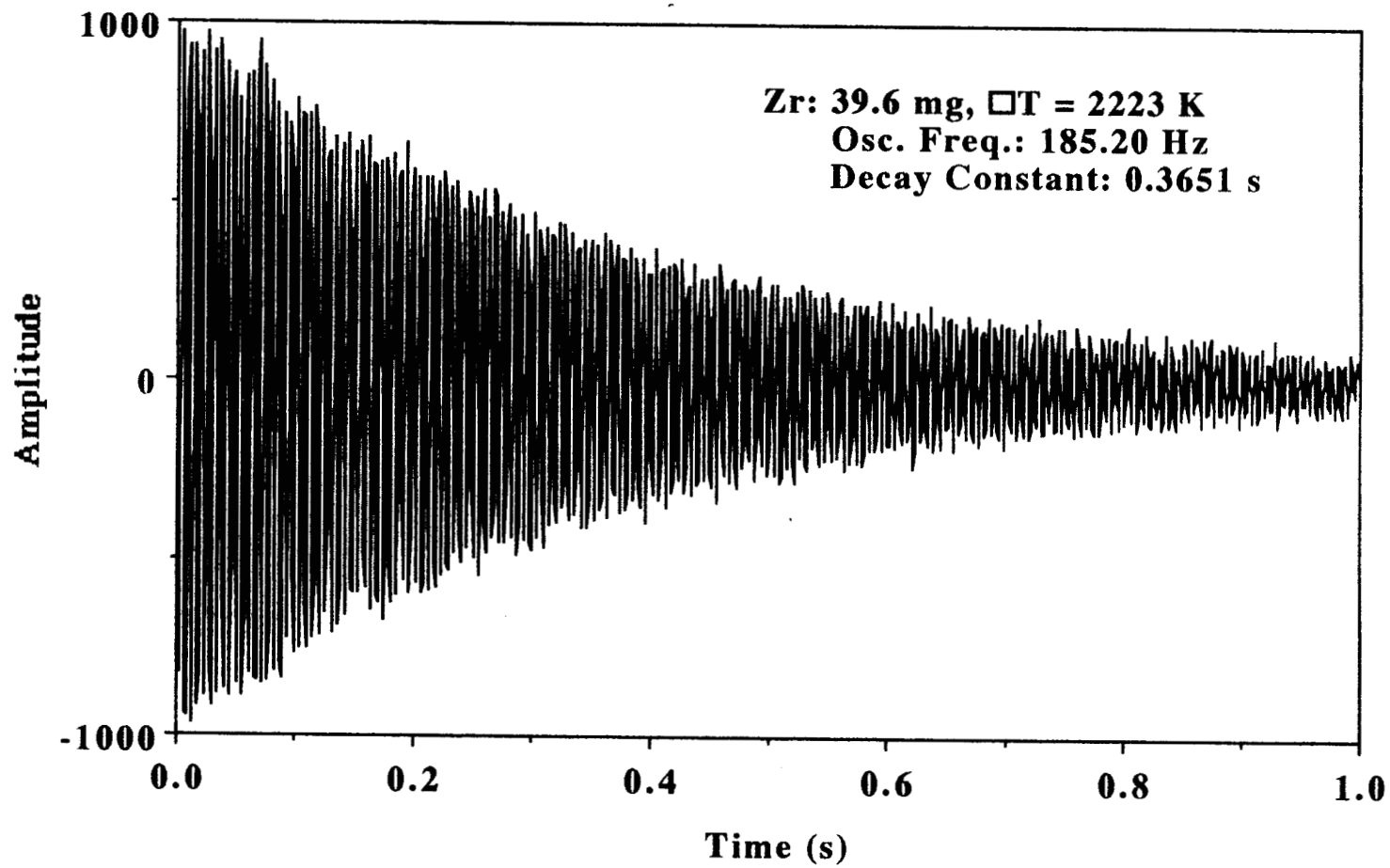
Fig. 3. Parab...

Fig. 4. Paradis et al

Zr: 39.6 mg, □T = 2223 K
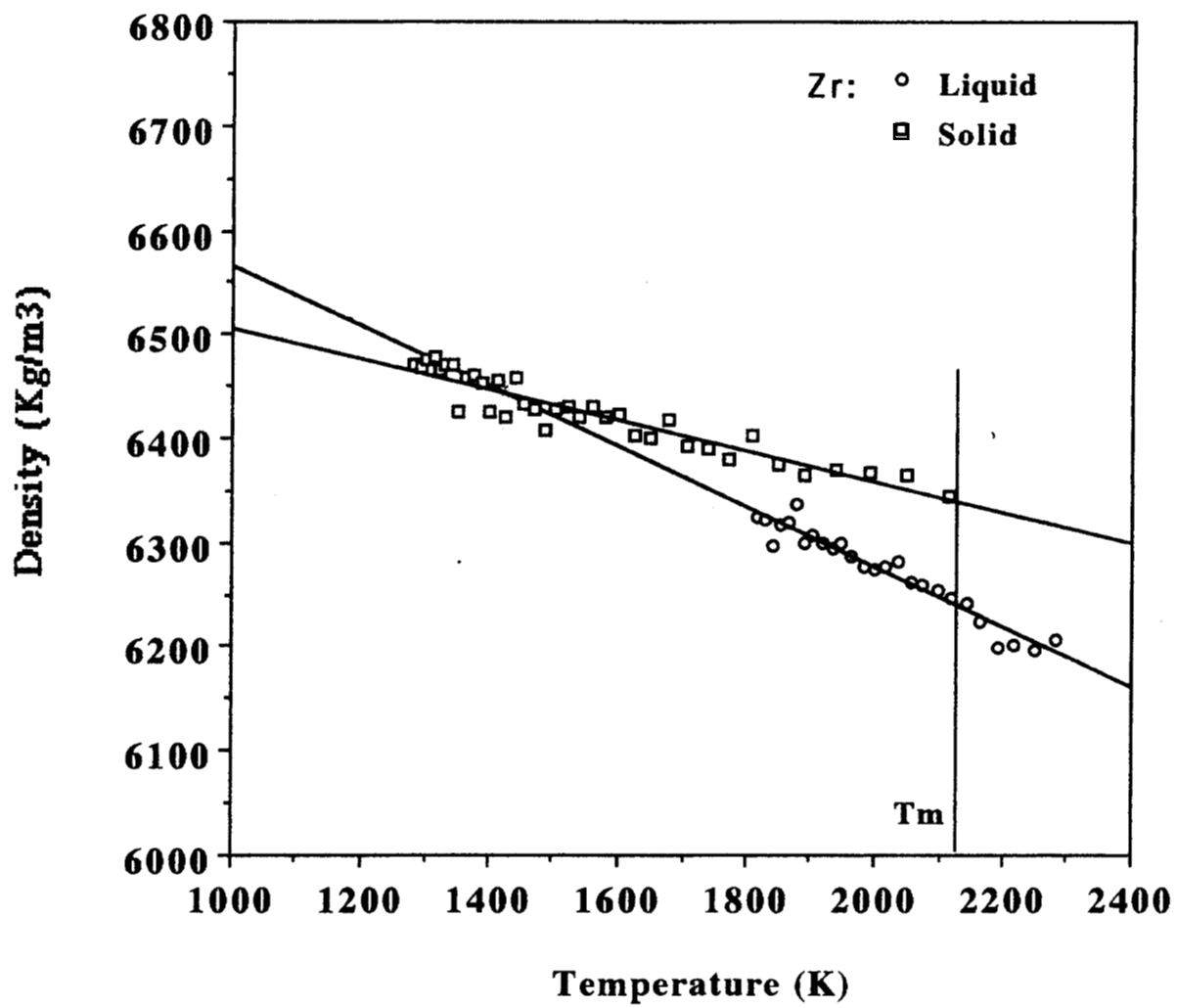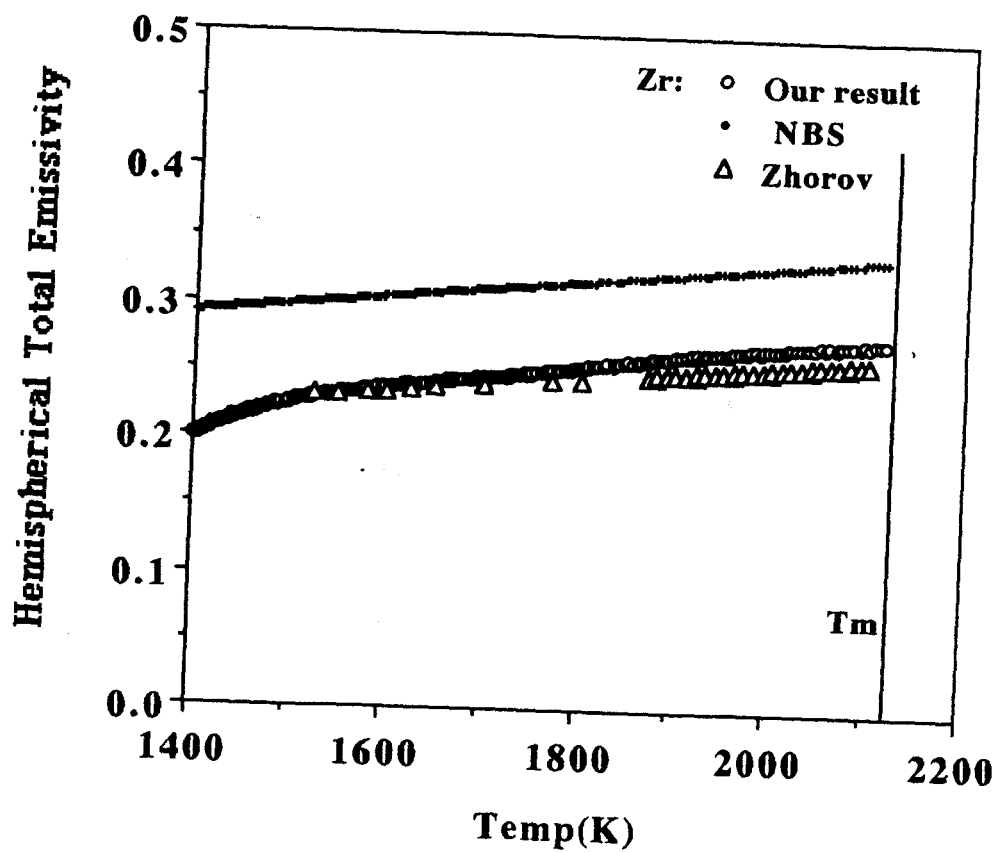Osc. Freq.: 185.20 Hz
Decay Constant: 0.3651 s

Fig 6. Paradis et al

Fig. 9, Paradis et al

Fig. 11. Paradis et al